

Silicon Nanocrystallites in SiO₂ Matrix: The Role of Disorder and Size

Roberto Guerra, Ivan Marri, Rita Magri, Layla Martin-Samos

CNR-INFM-S³ and Dipartimento di Fisica - Università di Modena e Reggio Emilia - via Campi 213/A I-41100 Modena Italy.

Olivia Pulci

European Theoretical Spectroscopy Facility (ETSF) and CNR-INFM, Dept. of Physics,
Università di Roma "Tor Vergata" Via della Ricerca Scientifica 1, I-00133 Roma, Italy

Elena Degoli and Stefano Ossicini

CNR-INFM-S³ and Dipartimento di Scienze e Metodi dell'Ingegneria - Università di
Modena e Reggio Emilia - via Amendola 2 Pad. Morselli, I-42100 Reggio Emilia Italy.

(Dated: September 3, 2010)

We compare, through first-principles pseudopotential calculations, the structural, electronic and optical properties of different size silicon nanoclusters embedded in a SiO₂ crystalline or amorphous matrix, with that of free-standing, hydrogenated and hydroxided silicon nanoclusters of corresponding size and shape. We find that the largest effect on the opto-electronic behavior is due to the amorphization of the embedded nanocluster. In that, the amorphization reduces the fundamental gap while increasing the absorption strength in the visible range. Increasing the nanocluster size does not change substantially this picture but only leads to the reduction of the absorption threshold, following the quantum confinement rule. Finally, through the calculation of the optical absorption spectra both in a independent-particle and many-body approach, we show that the effect of local fields is crucial for describing properly the optical behavior of the crystalline case while it is of minor importance for amorphous systems.

PACS numbers: 73.22-f; 71.24.+q, 73.20.at; 78.67.Bf.

I. INTRODUCTION

It is generally accepted that the quantum confinement (QC), observed when electron and hole are constrained in one or more dimensions by a potential well, is essential for the visible light emission in silicon nanoclusters (NCs)¹⁻³. Nevertheless, some open questions still exist. For instance, it is not yet known how much the QC model correctly describes the dependence of the energy gap E_G on the NC size and how structure distortions and surface properties can influence the band-gap value. Again, controversial interpretations of the photoluminescence (PL) microscopic origin in low-dimensional Si structures still exist. Surface effects, in particular oxidation⁴⁻⁶, on the NC optical properties have been addressed in the last years. Many theoretical⁷⁻⁹ and experimental⁷ works have proved that interface properties have dramatic effects on the emission spectra of NCs. Besides, the size of the NC is a crucial parameter^{10,11} to determine whenever such interface effects dominate (smaller NCs) or become negligible (larger NCs) respect to QC.

Various efforts have been done in order to describe optical absorption and emission spectra in such systems. In this context, inclusion of excitonic and many-body effects appears to be of fundamental importance¹². However, until now, no work has yet tackled the excitonic problem for this kind of systems due to the difficulty to deal with a large number of atoms.

In 2003 the first theoretical *ab-initio* calculation considering a small Si-NC embedded in a SiO₂ matrix^{13,14} has been published. In this work, both the host matrix

and the embedded nanostructure were fully relaxed.

In the present work a more detailed first-principles calculation of the structural, electronic and optical properties of Si-NC embedded in a SiO₂ matrix is reported. The two complementary cases of a perfectly crystalline and a completely amorphous system are taken into account. In particular, the effects generated by the surrounding matrix on the electronic properties of the NCs (of different size) are analyzed. The results are here compared with the corresponding ones of the free standing systems of same size.

The paper is organized as follows. A description of the theoretical methods and of the systems is given in section II. The structural, electronic and optical properties are analyzed in section III for both crystalline (section III A) and amorphous (section III B) cases. The effects of the NCs size are analyzed in sec. III C. The excited state properties described through many-body methods are reported in section IV. Conclusions are presented in section V.

II. THE METHOD

The β -cristobalite (BC) SiO₂ is well known to give rise to one of the simplest Si/SiO₂ interface because of its diamond-like structure¹⁵. The crystalline structure has been obtained from a Si₆₄O₁₂₈ cubic matrix (of size $L = 14.32 \text{ \AA}$) by removing all oxygens included in a sphere of radius 4.4 \AA placed at the center of the cubic supercell. The results is a structure of 64 Si and 116 O atoms with

10 Si bonded together to form a small crystalline skeleton with T_d local symmetry before relaxation. In such core, Si atoms show a larger bond length (3.1 Å) with respect to that of the Si bulk structure (2.35 Å). No defects (dangling bonds) are present, and all the O atoms at the Si/SiO₂ interface are single bonded with the Si atoms of the NC.

The optimized structure has been achieved by relaxing the total volume of the cell (see Fig. 1, left panel). This approach gives a correct description of the atomic average density in the NC region. Moreover, the small distortion induced in the host matrix (essentially due to the metastable nature of the BC) is practically irrelevant on the NC and the interface configuration. On the other hand, relaxation criteria based on a fixed supercell volume produce, when oxygens are removed, a strong reduction of the atomic average density, giving thus not realistic results. Together with the crystalline structure, the complementary case of an amorphous silica (a-SiO₂) has been considered. The glass model has been generated using classical molecular dynamics (MD) simulations of quenching from a melt, as described in Ref. ¹⁶. The simulations have been done using semi-empirical ionic potentials¹⁷, assuming an effective quench rate of $2.6 \cdot 10^{13}$ K/s. The glass match the well-connected definition of Zachariasen¹⁸. The amorphous dot structure has been obtained starting from a Si₆₄O₁₂₈ amorphous silica cell by removing the 10 oxygen atoms included in a sphere of radius 3.5 Å placed at the center of the cell, as shown in Fig. 1 (right panel). The relaxation of all the structures have been performed using the SIESTA code^{19,20} and Troullier-Martins pseudopotentials with non-linear core corrections. A cutoff of 38 Ry on the plane-wave basis set and no additional external pressure or stress were applied. Atomic positions and cell parameters have been left totally free to move.

Figure 2 shows the radial distribution function $g(r)$ of

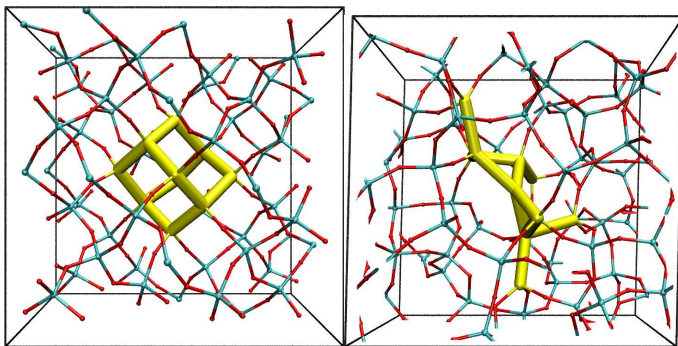


FIG. 1: (color online) Stick and ball pictures of the final optimized structure of Si₁₀ in β -cristobalite matrix (left panel) or in a-SiO₂ glass (right panel). Red (dark gray) spheres represent the O atoms, cyan (gray) spheres represent the Si of the matrix, and the yellow (gray) thick sticks represent the Si atoms of the NC.

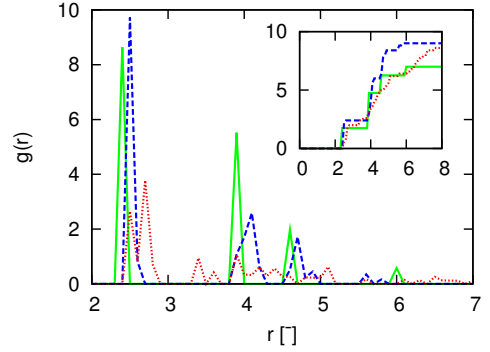


FIG. 2: (color online) Radial distribution function (and in the inset its integral) for the bulk silicon (green solid line), the crystalline Si₁₀ (blue dashed line) and amorphous a-Si₁₀ (red dotted line) NCs without the matrix contribution.

the crystalline (Si₁₀) and amorphous (a-Si₁₀) silicon NCs without considering the matrix contribution, compared with that of the NC made of the 8 atoms forming the primitive cubic cell of bulk silicon. In the inset the integrated radial distribution functions are shown. We note that the crystalline and the amorphous NCs present a nearest-neighbor distance of about 2.43 Å, strained respect to the typical Si-bulk value (2.35 Å), in fair agreement with the outcomes of Yilmaz et al.²¹. As expected, there is a good matching between the $g(r)$ of the crystalline NC and the Si-bulk case, while the long-range order is clearly broken in the amorphous system.

Electronic and optical properties of the relaxed structures have been obtained in the framework of DFT, using the ESPRESSO package²². Calculations have been performed using norm-conserving pseudopotentials within the LDA approximation with a Ceperley-Alder exchange-correlation potential, as parametrized by Perdew-Zunger. An energy cutoff of 60 Ry on the plane wave basis have been considered. To include the many-body corrections we have first calculated, starting from the DFT-LDA eigenvalues and eigenvectors, the GW²³ quasiparticle band structure using 10975 plane waves for the correlation part of the self-energy, and 20001 plane waves for the exchange part. The Bethe-Salpeter equation has been then solved considering an excitonic Hamiltonian made up of more than 65.000 transitions. The Haydock algorithm has been used to solve the Hamiltonian. Calculations have been performed using the EXC code²⁴.

III. INDEPENDENT-PARTICLE RESULTS

In parallel to the crystalline and amorphous Si₁₀/SiO₂ systems, three other structures have been studied: (i) the pure SiO₂ matrix (in the same phases as used for the embedded NC calculations), (ii) the isolated

NCs as extracted from the relaxed NC-silica complexes and capped by hydrogen atoms ($\text{Si}_{10}\text{-H}$), (iii) the NCs together with the first interface oxygens extracted as in point (ii), and then passivated by hydrogen atoms ($\text{Si}_{10}\text{-OH}$). In the last two cases only the hydrogen atoms have been relaxed. The goal is to distinguish between the properties that depend only on the embedded NC from those that are instead influenced by the presence of the matrix. The comparison of the results relative to different passivation regimes (H or OH groups) could give some insight on the role played by the interface region.

A. The crystalline cluster in β -cristobalite matrix

From the analysis of the relaxed $\text{Si}_{10}/\text{SiO}_2$ supercell emerges that the NC has a strained structure with respect to bulk Si^{21,25,26} (see Fig. 2), while the β -cristobalite matrix is strongly distorted near the NC and reduces progressively its stress far away from the interface²⁷. The electronic and optical properties of the relaxed structures of $\text{Si}_{10}/\text{SiO}_2$, SiO_2 bulk, $\text{Si}_{10}\text{-H}$ and $\text{Si}_{10}\text{-OH}$ have been computed. Figure 3 shows the comparison between the band structures (energy levels) of all these systems. We see, first of all, a strong reduction of the $\text{Si}_{10}/\text{SiO}_2$ energy gap ($E_G=1.77$ eV) with respect to both bulk SiO_2 (5.44 eV) and the isolated NC passivated by H atoms (4.66 eV); finally, as confirmed by Refs. 4,5,7, the passivation by OH groups tends to red-shift the energy spectrum ($E_G=1.6$

eV). The smaller gap with respect to the SiO_2 bulk case is clearly due to the formation of confined states within the NC, lying between the SiO_2 band edges, as displayed in Fig. 3a and 3b. These states are fundamentally different from those of the free-standing hydrogenated NC (Fig. 3c). In the embedded NC states, indeed, we find a strong contribution due to the presence of interfacial oxygen atoms. This is also confirmed by the resemblance

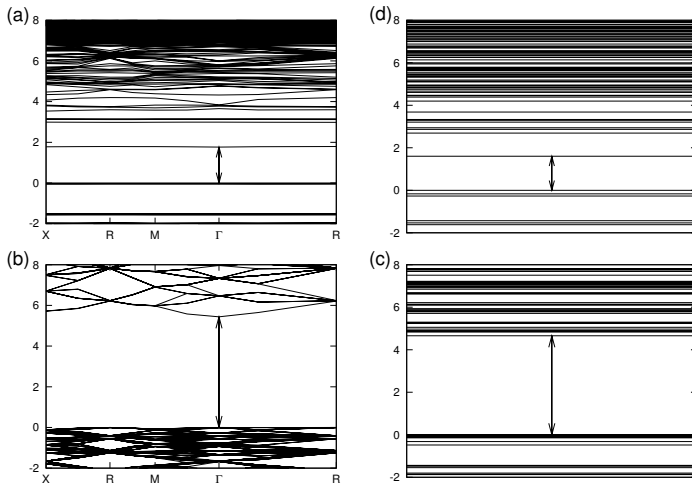


FIG. 3: Band structure along high symmetry points of the BZ for the crystalline Si_{10} NC in β -cristobalite (a), compared with the band structure of β -cristobalite bulk (b), the energy levels for the isolated Si_{10} NC passivated by H (c) and by OH groups (d). The arrows show the HOMO-LUMO band gap values. The units are in eV.

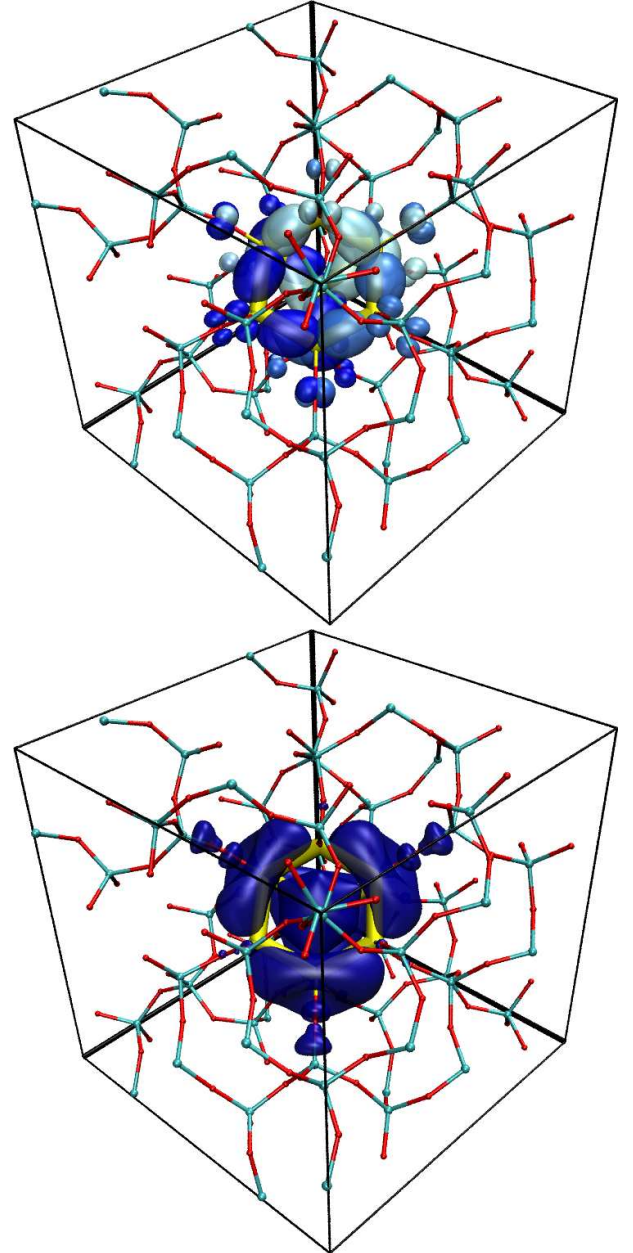


FIG. 4: (color online) Kohn-Sham orbitals at 10% of their max. amplitude for the Si_{10} crystalline embedded NC. Top panel: HOMO state is represented in blue (gray), HOMO-1 in azure (light gray), HOMO-2 in lightest blue (lightest gray). Bottom panel: LUMO is represented in dark blue (dark gray).

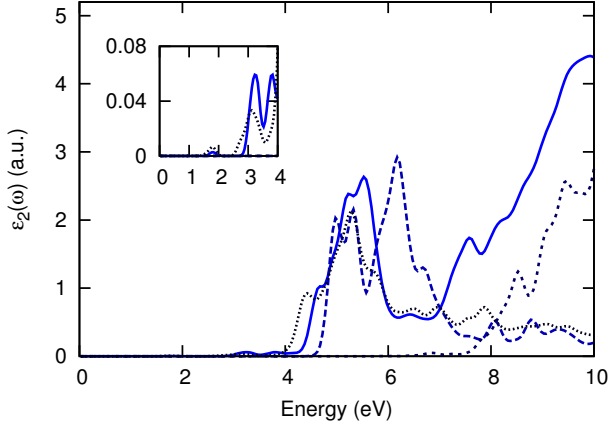


FIG. 5: (color online) DFT-RPA imaginary part of the dielectric function for the Si_{10} crystalline NC in β -cristobalite matrix (solid line) compared with that of isolated Si_{10} -H NC (long-dashed line), the β -cristobalite bulk (short-dashed line), and the Si_{10} -OH NC (dotted line). The inset shows an enlargement of the spectra at low energies.

existing between the gap values of the embedded NC and of the NC simply passivated by the OH groups (Fig. 3d). E_G is thus almost completely determined by the barrier provided by the first shell of oxygen atoms. The typical behavior of the bulk dispersed states is still recognizable far away from the band edges, where the NC influence tends to vanish. The square modulus contour plots of the highest occupied molecular orbital (HOMO) and the two states just below it (HOMO-1, HOMO-2), for the Si_{10} crystalline NC in the BC matrix are reported in Fig. 4. The supercell relaxation breaks the symmetry of the system, and consequently the degeneracy of the three states at the top of the valence band. Therefore these states present slightly different eigenvalues but preserve the character of the original symmetry. In accordance with Ref. 25, these states are mainly localized on part of the NC, in particular on the Si-Si bonds and on the interface oxygens, while the lowest unoccupied molecular orbital (LUMO) is localized on the interface and over all the entire NC region. It is clearly shown in Fig. 4 that the first shell of oxygens around the NC are able to completely trap the NC density charge, thus forming a strong barrier that is responsible for the QC effect.

In Figure 5 the imaginary part of the dielectric functions (calculated within the DFT-RPA approach, using the dipole approximation and neglecting the local-field (LF) effects) of $\text{Si}_{10}/\text{SiO}_2$, Si_{10} -H and Si_{10} -OH NCs, and of the BC bulk are reported. A detailed analysis of the results allows to identify three distinct zones in the spectra. The first one, above 6 eV, where the $\text{Si}_{10}/\text{SiO}_2$ and BC bulk are very similar. The second one, between ~ 4 eV and ~ 6 eV, where a clear contribution due to the embedded Si-NC is present. The third one, below 4 eV, where

	SiO_2	$\text{Si}_{10}/\text{SiO}_2$	Si_{10} -OH	Si_{10} -H
Crystalline	5.44	1.77	1.60	4.66
Amorphous	5.40	1.41	1.55	1.87

TABLE I: DFT HOMO-LUMO gap values (in eV) for the crystalline and amorphous silica, embedded, OH-terminated, H-terminated Si_{10} NC.

the transitions can not be ascribed neither to the matrix region nor to the pure NC. In this region the peaks are originated by the interplay between the embedded NC and the matrix; in particular they are due to the presence of the oxygen atoms located at the interface region. This is confirmed by the similarity that exists, in this energy region, between the $\text{Si}_{10}/\text{SiO}_2$ and the Si_{10} -OH spectra, as depicted in the insertion of Fig. 5. The presence of OH groups thus induces a complex structure in the part of the spectrum below 4 eV that can be compared with the peaks of the $\text{Si}_{10}/\text{SiO}_2$ structures.

B. The amorphous cluster in a glass

The NC, when formed in the glass, completely loses memory of the starting tetrahedral symmetry (as shown in the previously discussed Fig. 2). No dangling bonds are present at the NC surface while some bridge-bonded oxygens appear (that are not present in the crystalline case). Despite the fact that the dra-

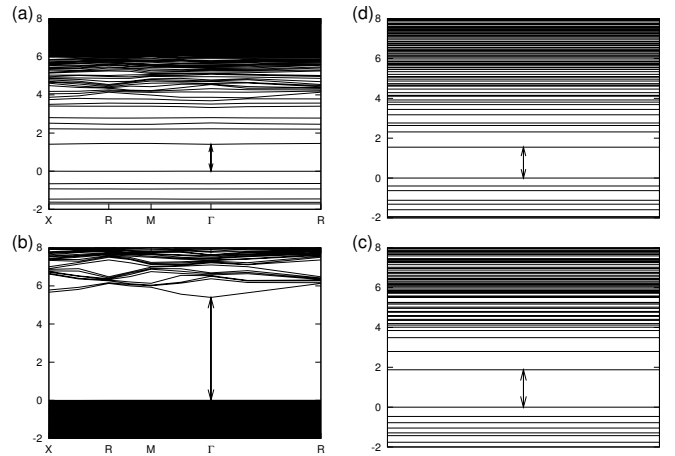


FIG. 6: Band structure along high symmetry points of the BZ for the a- $\text{Si}_{10}/\text{a-SiO}_2$ system (a) compared with the band structure of the glass bulk (b), the energy levels for the isolated a- Si_{10} NC passivated by H (c) and by OH groups (d). The arrows show the HOMO-LUMO band gap values. The units are in eV.

matic structural changes with respect to the crystalline case, similar considerations can be done concerning the optoelectronic properties. While the amorphization process does not affect the behavior of the glass matrix, it strongly reduces the energy gap of the isolated a-Si₁₀-H NC, of the a-Si₁₀-OH NC, and of the composite a-Si₁₀/a-SiO₂ system (see Fig. 6). The HOMO-LUMO gaps are summarized in table I.

We note that, contrary to the crystalline case, the amorphous hydroxided NC shows a gap value slightly greater

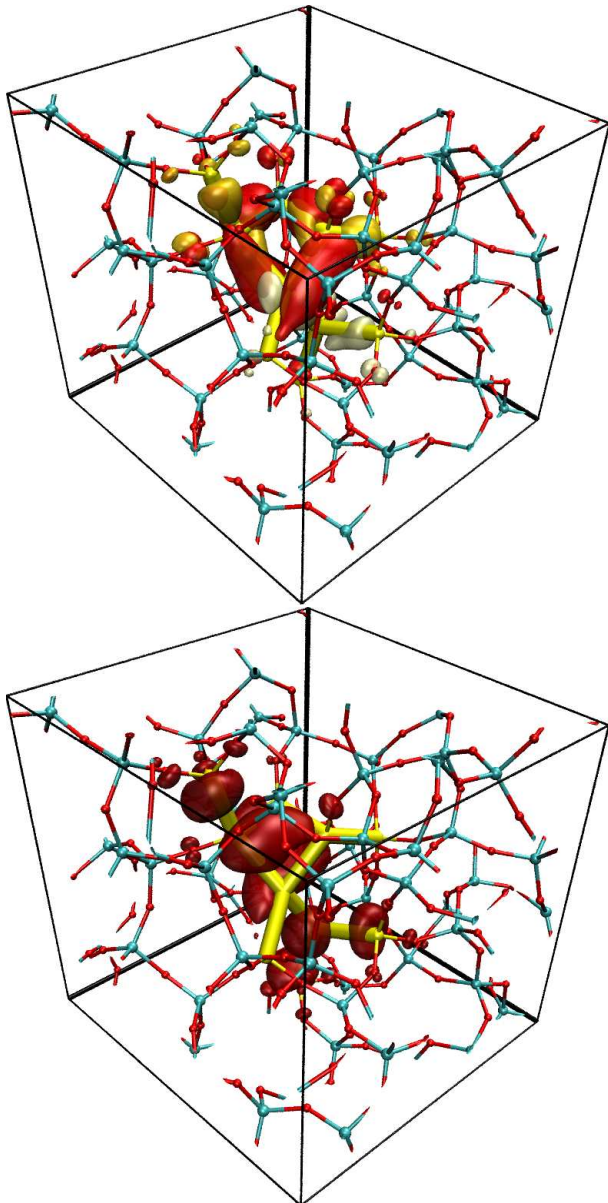


FIG. 7: (color online) Kohn-Sham orbitals at 10% of their max. amplitude for the a-Si₁₀ amorphous embedded NC. Top panel: HOMO state is represented in red (gray), HOMO-1 in orange (light gray), and HOMO-2 in white. Bottom panel: LUMO is represented in dark red (dark gray).

than when embedded. Also in this case the states at the valence and conduction band edges are localized at the interface; in particular they stem from the OH passivation. Obviously the reduction of the local symmetry induces a splitting in the energy levels and, as a consequence, a more uniform distribution of states.

The HOMO, HOMO-1, HOMO-2 and LUMO states (see Fig. 7) follow the shape of the NC, resulting strongly deformed with respect to the crystalline case, but are still clearly confined by the interface oxygen shell.

In the calculated optical absorption spectra (see Fig. 8) the three regions due to the hosting matrix, Si-NC, and interface, are still clearly distinguishable.

The most important differences between the calculated optical absorption spectra for both the amorphous and the crystalline embedded NCs are found in the energy range between 2 and 4 eV. In this region the amorphous system shows more intense peaks with respect to the crystalline case, suggesting a possible higher emission in the visible range.

Despite the fact that the possibility to form amorphous NC in silica has been recently explored²⁸, experimental measurements on single Si-NCs with diameters of the order of 1 nm have not yet been performed. Thus, a straightforward comparison of our results with experimental data is not possible. Besides, the comparison with other works²⁹ sustains the idea that the strong deformation of the NC is determinant for the absorption strength at low energies. This idea is also supported by the fact that, for larger systems, when the shape of the NCs tends to be spherical and the distortion is usually less pronounced^{11,30}, crystalline and amorphous systems

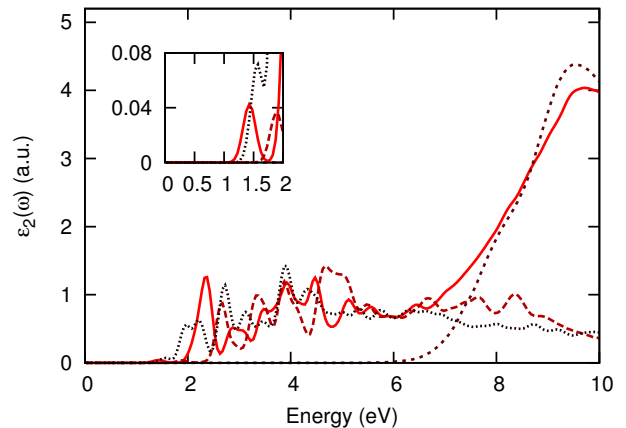


FIG. 8: (color online) DFT-RPA imaginary part of the dielectric function for the a-Si₁₀ NC in a glass matrix (solid line) compared with that of isolated, hydrogenated a-Si₁₀-H NC (long-dashed line), the glass matrix (short-dashed line), and the hydroxided a-Si₁₀-OH NC (dotted line). The inset shows an enlargement of the spectra at low energies.

produce more similar absorption spectra. This topic will be discussed in the next subsection.

C. Size Effects

From a theoretical point of view, the simplest model for the QC is provided by the particle-in-a-box scheme, in which the box size is given by the NC diameter and the potential barrier represents the host insulating matrix. When QC effect dominates over other quantum phenomena, for an infinite barrier potential, we have $E_G(R) = \epsilon_G + A/R^\alpha$, where ϵ_G is the bulk-silicon band gap, R is the radius of the NC, A is a positive constant and $\alpha \leq 2$ ³¹. This model, however, is often too simple to describe correctly the experimental results.

Experimentally, several factors contribute to make the interpretation of measurements of the optical gaps a difficult task. For instance, samples show a certain distribution in the NC size, that is difficult to be determined. In this case it is possible that the observed PL peak does not correspond exactly to the mean size but instead to the largest PL rate. Again, NC synthesized by using different techniques often show different properties in size, shape and in the interface structure. Finally, also the NC-NC interactions can play a significant role on the emission spectrum.

Recent measurements on samples with diameters in the range of 2-10 nm have reported³²⁻³⁸ a PL peak that is blue-shifted by $\Delta E_G(R) \sim R^{-\alpha}$, with $1 < \alpha < 1.5$. Thus, the model described above is far from being able to reproduce the measurements. In order to improve it, the finiteness of the potential barrier and also other corrections should be taken into account. For example, the inclusion of the electron-hole Coulomb interaction, that contributes a further R^{-1} dependence in blue-shifting the energy, results in a more gradual dependence of the op-

tical gap on the dot radius, as observed experimentally. As mentioned above, our investigation explores the small dot size limit, with a diameter range within 1 nm. In this range, most of the NC atoms are positioned at the interface, where the effects of stress and oxidation are stronger. For bigger NCs, when Si-bulk states emerge and the surface-to-volume ratio decreases, these effects are limited; in this case we expect a response that is independent of the specific geometrical configuration. Thus, in order to understand all the interface-related phenomena, an investigation of the small size limit becomes necessary.

To model NC of increasing size, we enlarge the hosting matrix so that the separation between NCs is still around 1 nm, that we consider enough to correctly describe the stress localized around each NC and to avoid an overlapping of the NC states that can be caused by the application of the periodic boundary conditions¹³. These considerations lead us to choose a BC matrix of 648 atoms (in a cubic cell with lattice parameter of 2 nm) with a core of 32 silicon atoms, having an average diameter of 1 nm. The relaxed Si₃₂ NC shows a strained interface with average Si-Si bond-lengths of 2.6 Å, while the silicon atoms in the core have a less strained bond-length of 2.43 Å. Note that Si₁₀/SiO₂ and Si₃₂/SiO₂ have approximatively the same ratio between the NC and the matrix volumes. The amorphous embedded a-Si₃₂ NC is again produced by MD annealing and successive *ab-initio* relaxation. The final structures are shown in Fig. 9. Once more, bridge-bonded oxygens are present at the interface and we find that the number of Si-O-Si bonds increases with the dimension of the NC (8 bonds in this case with respect to the 3 present in the smaller NC) in nice agreement with previous results obtained by different methods^{11,39}.

E_G values calculated in DFT for Si₃₂/SiO₂, Si₃₂-OH and Si₃₂-H structures are reported in Tab. II. We can note that, while E_G of Si₃₂-H is smaller with respect to Si₁₀-H due to the QC, for the other structures it strongly depends on the interface configuration. As a consequence, for both the Si₃₂/SiO₂ and Si₃₂-OH systems, E_G increases when the phase is crystalline, and decreases when the corresponding structures are amorphous. We note that, while the amorphous systems present interfaces where several types of oxidations and coordination levels coexist, the crystalline case presents a situation in which all the interface O atoms are single-bonded with the Si-NC atoms. Specifically, the Si-atoms at the inter-

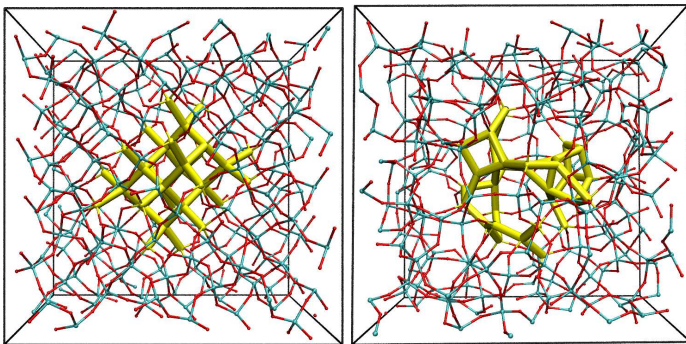


FIG. 9: (color online) Stick and ball pictures of the final optimized structure of Si₃₂ NC in a β -cristobalite matrix (left) and a-Si₃₂ NC in a a-SiO₂ glass (right). Red (dark gray) spheres represent the O atoms, cyan (gray) spheres represent the Si of the matrix, and the yellow (gray) thick sticks represent the Si atoms of the NC.

	Si ₃₂ /SiO ₂	Si ₃₂ -OH	Si ₃₂ -H
Crystalline	2.62	2.15	2.78
Amorphous	1.19	0.99	1.59

TABLE II: DFT HOMO-LUMO gap values (in eV) for the crystalline and amorphous silica, embedded, OH-terminated, H-terminated Si₃₂ NC.

face of the $\text{Si}_{10}/\text{SiO}_2$ and $\text{Si}_{32}/\text{SiO}_2$ systems are respectively bonded with 1.6 and 2.8 oxygens in average. It is worth to note that a recent size-dependent experimental study of Si 2*p* core-level shift at Si-NC/SiO₂ interface showed that the shell region around the Si-NC bordered by SiO₂ consists of the three Si suboxide states, Si^{1+} , Si^{2+} , and Si^{3+} , whose densities strongly depend on the NC size⁴⁰. Generally, such oxydation degree is responsible for two, competitive, major effects on E_G : while from one side a higher oxydation increases E_G , from the other side it produces a higher strain on the Si-NC atoms that results in a reduction of E_G . Briefly, what emerges is that these two contributions are approximately of the same order of magnitude, and the dominance of one over the other is strictly dependent on the considered system (a publication on this topic is currently under development).

In our case, after performing a full relaxation, in order to remove the strain, of the $\text{Si}_{10}\text{-OH}$ and $\text{Si}_{32}\text{-OH}$ structures we still obtain an E_G difference of about 1 eV. Thus, the increased E_G of the larger system can be referred to the greater amount of oxydation of the interface silicon atoms.

The analysis of the valence and conduction band edge

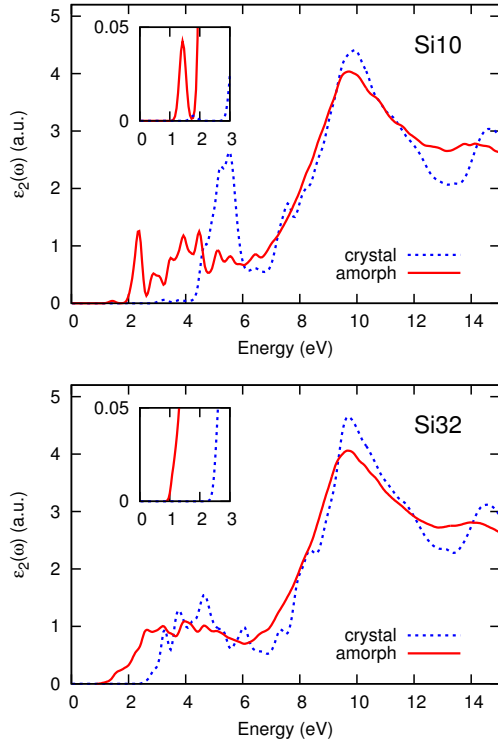


FIG. 10: (color online) DFT-RPA imaginary part of the dielectric function for the crystalline (dotted) and amorphous (solid) Si_{10} (upper) and Si_{32} (lower) embedded NCs. The insets show an enlargement of the spectra at low energies.

states of the $\text{Si}_{32}/\text{SiO}_2$ system, points out that the former are essentially localized in a well defined part of the NC, near the interface zone, while the latter are localized on the whole volume (from the center to the interface) of the embedded structure.

The effects induced by the amorphization process on the optical properties of both $\text{Si}_{10}/\text{SiO}_2$ and $\text{Si}_{32}/\text{SiO}_2$ systems are depicted in Fig. 10, where the calculated absorption spectra for both crystalline (blue line) and amorphous (red line) phases are reported. Here we note that, while in the smaller $\text{Si}_{10}/\text{SiO}_2$ system the amorphization produces a net change in the shape of the spectrum below 6 eV, inducing also new strong structures in the energy windows between 2 and 4 eV, for the bigger $\text{Si}_{32}/\text{SiO}_2$ it seems to induce only a simple red-shift. These facts enforce our previous hypothesis that for bigger NCs the particular configuration of the interface becomes less important. This is especially true for the amorphous systems, where the diversity of the atomic configurations tend to average out the final properties. In order to compare theoretical and experimental results for the energy gap dependency, we introduce a new quantity, E_G^o , which is defined as the optical absorption threshold when all the transitions with an intensity lower than 1% of the highest peak are neglected. In this way we introduce a sort of "instrument resolution" by neglecting very low oscillator strength optical transitions (for instance the HOMO-LUMO transition in the $\text{Si}_{10}/\text{SiO}_2$ crystalline system). The obtained DFT E_G^o values for the embedded systems are depicted in Fig. 11. Here E_G^o has been calculated for Si-NC containing 2, 5, 10 and 32 atoms. It is clear that, while the increasing of the NC size always results in a reduction of E_G^o , the effect of the amorphization is to

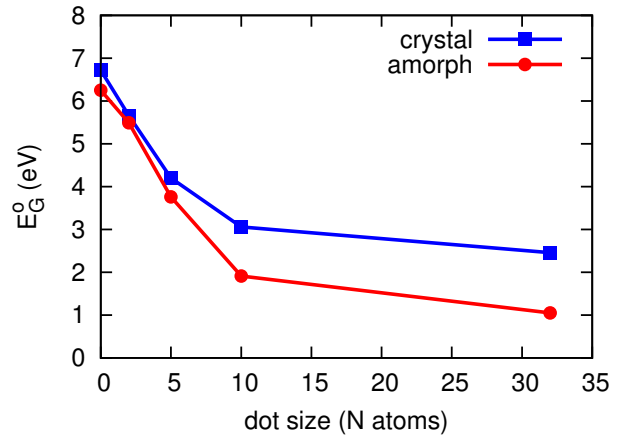


FIG. 11: (color online) E_G^o versus the Si-NC size and amorphization (embedded systems). $N=0$ corresponds to the pure silica, $N=32, 10, 5, 2$ correspond to an average diameters of, 1.0, 0.7, 0.45, 0.24 nm, respectively. The lines are drawn to guide the eye.

introduce an additional red-shift that becomes relevant for large NCs. For large number of atoms N we expect however a vanishing of the red-shift due to the fact that, for semiconductors, the main optical properties should only depend on the short range-order⁴¹.

IV. EXCITONIC AND MANY-BODY CORRECTIONS

Self-Energy and excitonic effects are known to play a very important role both in low dimensional systems (as the quantum dots) and in 3-dimensional systems as the SiO_2 . In this last case it is known that DFT underestimates the electronic gap of about 5 eV, and important excitonic effects are responsible of the strong absorption peak at about 10 eV. The inclusion of the many-body effects is thus of fundamental importance in order to obtain a better description of the optical properties of NCs embedded in SiO_2 . Quasi-particle effects within the GW approach⁴² and excitonic effects within the BS equation⁴³ have been considered in the calculation of the $\text{Si}_{10}/\text{SiO}_2$ electronic properties. Table III shows the calculated E_G within DFT, GW, GW+BSE+LF approximations. It is possible to observe that, in the ordered (amorphous) case, the inclusion of the GW corrections opens up the gap by about 1.9 (1.7) eV, while the excitonic and LF correction reduces it by about 1.5 (1.6) eV. Thus, the total correction to the LDA E_G results to be of the order of 0.4 (0.1) eV. We note that the final E_G of the crystalline and amorphous embedded NCs are quite different, i.e. 2.17 and 1.51 eV, respectively.

The difference between the GW electronic gap and the GW+BSE+LF optical excitonic gap gives the exciton binding energy E_b . Our calculated exciton binding energies are quite large: 1.5 eV (crystalline) and 1.6 eV (amorphous). They are very large if compared with that of bulk SiO_2 (almost 0 eV)^{44–46}, bulk Si (~ 15 meV) or with carbon nanotubes^{47,48} where $E_b \sim 1$ eV, but they are similar to those calculated for undoped and doped Si-NC^{49,50} of similar size and for Si and Ge small nanowires^{51,52}.

Fig. 12 shows the calculated DFT-RPA, GW+BSE+NLF, and GW+BSE+LF absorption spectra for the embedded Si_{10} and a- Si_{10} NCs. The results show that the inclusion of the many-body effects does not substantially modify the absorption spectra. In both cases the energy position of the absorption onset

	DFT	GW	GW+BSE+LF
Crystalline	1.77	3.67	2.17
Amorphous	1.41	3.11	1.51

TABLE III: Many-body effects on the gap values (in eV) for the crystalline and amorphous embedded Si_{10} dots.

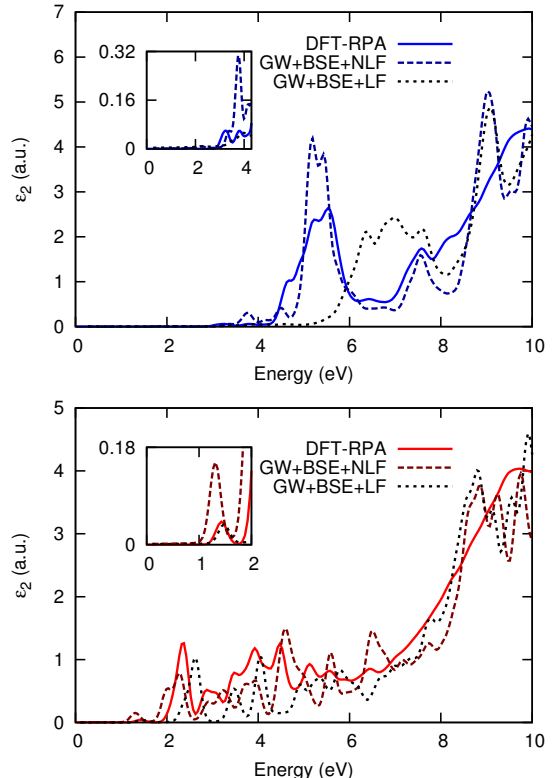


FIG. 12: (color online) DFT-RPA, GW+BSE+NLF (that is, without local fields), and GW+BSE+LF (with local fields) calculated imaginary part of the dielectric function for crystalline (top) and amorphous (bottom) case.

is practically not modified (see insets). Delerue and coworkers⁵³ found that, for Si-NC larger than 1.2 nm, the self-energy and Coulomb corrections almost cancel each other. In our case (about 0.7 nm), this cancellation does not completely occur, especially for the crystalline system, where self-energy effects dominate. Finally, we note that the inclusion of LF contributions has dramatic effects on the spectrum of the crystalline system, especially in the region between 4 and 6 eV, while the amorphous system seems to be affected by a simple blue-shift of the absorption threshold.

V. CONCLUSIONS

Considering as the β -cristobalite phase of the SiO_2 , like as the amorphous phase obtained by classical molecular-dynamics, we have generated silicon nanoclusters of different size and shape, that are embedded in a silica matrix. The final structures, that have been relaxed with the SIESTA method¹⁹, shows that the surrounding matrix always produces some strain on the nanocluster, especially at the Si/ SiO_2 interface. Then we have compared

the electronic and optical properties of the embedded structures, calculated within the DFT-LDA, with that of the free H- and OH- terminated clusters, and that of the pure silica. What emerges is that the electronic and optical behavior is strongly influenced by the structural properties of the considered systems; actually, apart for the quantum confinement effect on the energy gap due to the different NCs size, the amorphization of the embedded NC is responsible for the main electronic and optical changes of the whole system.

For the smaller cases, we have also investigated the local field, self energy, and binding energy effects. Concerning the optical properties we have shown that, while the

many body approach provides only minor corrections, the inclusion of local fields is crucial in the analysis of highly symmetric systems (crystalline case) but it is of minor importance in disordered structures (amorphous case).

This work shows that it could be worthy to experimentally investigate the optical properties of the matrix embedded amorphous nanoclusters^{54,55}, that show different properties with respect to their crystalline counterparts. This work is supported by PRIN2007 and CNR Italia-Turchia. We acknowledge CINECA CPU time granted by INFM (Progetto Calcolo Parallelo). We thanks A. Pedone for the contribution with the modelling of the silica glasses.

-
- ¹ L. Pavesi, L. Dal Negro, C. Mazzoleni, G. Franzó, F. Priolo, *Nature* **408**, 440 (2000).
 - ² S. Ossicini, L. Pavesi, F. Priolo, "Light Emitting Silicon for Microphotronics", Springer Tracts on Modern Physics **194**, Springer-Verlag Berlin (2003).
 - ³ O. Bisi, S. Ossicini, L. Pavesi, *Surf. Sci. Reports* **38**, 5 (2000).
 - ⁴ L. Ramos, J. Furthmüller, F. Bechstedt, *Appl. Phys. Lett.* **87**, 143113 (2005).
 - ⁵ L. Ramos, J. Furthmüller, F. Bechstedt, *Phys. Rev. B* **71**, 035328 (2005).
 - ⁶ P. Avramov, A. Kuzubov, A. Fedorov, P. Sorokin, F. Tomilin, Y. Maeda, *Phys. Rev. B* **75**, 205427 (2007).
 - ⁷ M. V. Wolkin, J. Jorne, P. M. Fauchet, G. Allan, C. Delerue, *Phys. Rev. Lett.* **82**, 000197 (1999).
 - ⁸ M. Luppi, S. Ossicini, *J. Appl. Phys.*, **94**, 2130 (2003).
 - ⁹ Z. Zhou, L. Brus, R. Friesner, *Nano Lett.* **3**, 163 (2003).
 - ¹⁰ G. Hadjisavvas, P.C. Kelires, *Phys. Rev. Lett.* **93**, 226104 (2004).
 - ¹¹ G. Hadjisavvas, P.C. Kelires, *Physica E* **38**, 99 (2007).
 - ¹² E. K. Chang, M. Rohlfing, S. G. Louie, *Phys. Rev. Lett.* **85** 2613 (2000).
 - ¹³ N. Daldosso, M. Luppi, S. Ossicini, E. Degoli, R. Magri, G. Dalba, P. Fornasini, R. Grisenti, F. Rocca, L. Pavesi, S. Boninelli, F. Priolo, C. Spinella, F. Iacona, *Phys. Rev. B* **68**, 085327 (2003).
 - ¹⁴ M. Luppi, S. Ossicini, *Phys. Rev. B* **71**, 035340 (2005).
 - ¹⁵ H. Kageshima, K. Shiraishi, in: M. Scheffler, R. Zimmermann (Eds.), *Proc. 23rd Int. Conf. Phys. Semicon.*, World Scientific, Singapore, p. 903, (1996).
 - ¹⁶ L. Martin-Samos, Y. Limoge, J.-P. Crocombette, G. Roma, N. Richard, E. Anglada, E. Artacho *Phys. Rev. B* **71**, 014116 (2005).
 - ¹⁷ B. W. H. van Beest, G. J. Kramer, R. A. van Santen, *Phys. Rev. Lett.* **64**, 1955 (1990).
 - ¹⁸ W. H. Zachariasen, *J. Am. Chem. Soc.* **54**, 3841 (1932).
 - ¹⁹ P. Ordejón, E. Artacho, J. M. Soler, *Phys. Rev. B (Rapid Comm.)* **53**, R10441 (1996).
 - ²⁰ J. M. Soler, E. Artacho, J. D. Gale, A. García, J. Junquera, P. Ordejón, D. Sánchez-Portal, *J. Phys.: Condens. Matt.* **14**, 2745 (2002).
 - ²¹ D. E. Yilmaz, C. Bulutay, T. Cagin, *Phys. Rev. B* **77**, 155306 (2008).
 - ²² www.pwscf.org
 - ²³ R. Del Sole, L. Reining, R. W. Godby, *Phys. Rev. B* **49** 8024 (1994).
 - ²⁴ www.bethe-salpeter.org
 - ²⁵ P. Kroll, H. J. Schulte, *Phys. Stat. Sol. B* **243** (2006).
 - ²⁶ D. E. Yilmaz, C. Bulutay, T. Çağın, *Phys. Rev. B* **77**, 155306 (2008).
 - ²⁷ T. Watanabe, K. Tatsamura, I. Ohdomari, *Appl. Surf. Science* **237**, 125 (2004).
 - ²⁸ F. Djurabekova, M. Backman, K. Nordlund, *Nuclear Instruments and Methods B* **266**, 2683 (2008).
 - ²⁹ C. Bulutay, *Phys. Rev. B* **76**, 205321 (2007).
 - ³⁰ F. Djurabekova, K. Nordlund, *Phys. Rev. B* **77**, 115325 (2008).
 - ³¹ V.A. Belyakov, V.A. Burdov, R. Lockwood, A. Meldrum, *Adv. in Opt. Tech.* 279502 (2008).
 - ³² J. De la Torre, A. Souifi, A. Poncet, G. Bremond, G. Guillet, B. Garrido, J. R. Morante, *Solid-State Electronics* **49** 1114 (2005).
 - ³³ X. Duan, C. M. Lieber, *Adv. Mater. (Weinheim, Ger.)* **12**, 298 (2000).
 - ³⁴ Y. Kanzawa, T. Kageyama, S. Takeda, M. Fujii, S. Hayashi, K. Yamamoto, *Solid State Commun.* **102**, 553 (1997).
 - ³⁵ S. Guha, B. Qadri, R. G. Musket, M. A. Wall, T. Shimizu-Iwayama, *J. Appl. Phys.* **88**, 3954 (2000).
 - ³⁶ S. Takeoka, M. Fujii, S. Hayashi, *Phys. Rev. B* **62**, 16820 (2000).
 - ³⁷ K. Watanabe, M. Fujii, S. Hayashi, *J. Appl. Phys.* **90**, 4761 (2001).
 - ³⁸ E. Lioudakis, A. Antoniou, A. Othonos, C. Christofides, A. G. Nassiopoulou, Ch. B. Lioutas, N. Frangis, *J. Appl. Phys.* **102** 083534 (2007).
 - ³⁹ M. Ippolito, S. Meloni, L. Colombo, *Appl. Phys. Lett.* **93**, 153109 (2008).
 - ⁴⁰ S. Kim, M. C. Kim, S.-H. Choi, K. J. Kim, H. N. Hwang, C. C. Hwang, *Appl. Phys. Lett.* **91**, 103113 (2007).
 - ⁴¹ J. Tauc, A. Abraham, L. Pajasova, R. Grigorovici, A. Vancu, *Non-Crystalline Solids*, p. 606, North-Holland Amsterdam (1965).
 - ⁴² L. Hedin, *Phys. Rev.* **139**, A796 (1965).
 - ⁴³ G. Onida, L. Reining, A. Rubio, *Rev. of Mod. Phys.* **74**, 601 (2002).
 - ⁴⁴ E. K. Chang, M. Rohlfing, S. G. Louie, *Phys. Rev. Lett.* **85**, 2613 (2000).
 - ⁴⁵ A. Marini, R. Del Sole, A. Rubio, *Phys. Rev. Lett.* **91**, 256402 (2003).

- ⁴⁶ L. E. Ramos, J. Furthmüller, F. Bechstedt, Phys. Rev. B **69**, 085102 (2004).
- ⁴⁷ C. D. Spataru, S. Ismail-Beigi, L. X. Benedict, S. G. Louie, Phys. Rev. Lett. **92**, 077402 (2004).
- ⁴⁸ E. Chang, G. Bussi, A. Ruini, E. Molinari, Phys. Rev. Lett. **92**, 196401 (2004).
- ⁴⁹ E. Luppi, F. Iori, R. Magri, O. Pulci, S. Ossicini, Elena Degoli, V. Olevano, Phys. Rev. B **75**, 033303 (2007).
- ⁵⁰ F. Iori, E. Degoli, R. Magri, I. Marri, G. Cantele, D. Ninno, F. Trani, O. Pulci, S. Ossicini, Phys. Rev. B **76**, 085302 (2007).
- ⁵¹ M. Bruno, M. Palummo, A. Marini, R. Del Sole, V. Olevano, A. N. Kholod, S. Ossicini, Phys. Rev. B **72**, 153310 (2005).
- ⁵² M. Bruno, M. Palummo, A. Marini, R. Del Sole, S. Ossicini, Phys. Rev. Lett. **98**, 036807 (2007).
- ⁵³ C. Delerue, M. Lannoo, G. Allan, Phys. Rev. Lett. **84**, 2457 (2000).
- ⁵⁴ L. Pavesi and G. Guillot, in Optical Interconnects: The Silicon Approach, edited by W. Rhodes (Springer, Berlin, 2006).
- ⁵⁵ L. Khriachtchev, T. Nikitin, C. J. Oton, R. Velagapudi, J. Sainio, J. Lahtinen, S. Novikov, J. Appl. Phys. **104**, 104316 (2008).